J Nanostruct 13(2): 359-372, Spring 2023

RESEARCH PAPER

Synthesis and Characterization of Fe_3O_4/TiO_2/Ag Magnetic Nanocomposite with Enhanced Photocatalytic Activity for Methylene Blue Degradation and Modeling by an Artificial Neural Network (ANN)

*Saghar Jarollahi [1], Gholamreza Nabiyouni [2,3], Ziba Sorinezami [4 *], Ali Shabani [2,3]*

[1] *Department of Science, Arak University of Technology, Arak, Iran*

[2] *Department of Physics, Faculty of Science, Arak University, Arak, 38156-88349, Iran*

[3] *Institute of Nanoscience and Nanotechnology, Arak University, Arak, Iran*

[4] *Department of Chemistry, University of Zabol, Zabol, Iran*

ARTICLE INFO

Article History:
Received 24 December 2022
Accepted 17 March 2023
Published 01 April 2023

Keywords:
ANN
LSPR
Magnetic properties
Nanocomposite
Photocatalyst

ABSTRACT

Increasing environmental pollution is one of the major problems in recent decades. Finding new ways to remove contaminants is critical mission for scientists. In this research, Fe_3O_4/TiO_2/Ag magnetic nanocomposite synthesized for investigation of degradation of methylene blue (MB). Fe_3O_4 magnetic nanoparticles was first synthesized with simple co-precipitation method. Then the magnetic nanocomposite structure of Fe_3O_4/TiO_2 by hydrothermal methodwas shaped. After that, to improve the ability of the nanocomposite to reduction of MB, Ag nanoparticles was doped on the surface of the Fe_3O_4/TiO_2. In fact, in this structure, we used local surface plasmon resonance (LSPR) future of Ag and photocatalyst property of TiO_2 to modify the ability of MB reduction. Various techniques were employed to characterize the morphology of magnetic nanocomposite such as X-ray diffractometer (XRD), Fourier transform infrared spectroscopy (FT-IR), scanning electron microscope (SEM) and an alternating gradient force magnetometer (AGFM). We also used ultraviolet-visible (UV) analyses to determine the band gap. The results show that the nanocomposite formed successfully in desired structure and morphology. Catalytic measurements on the samples show an excellent efficiency for the MBdegradation. After the reduction of MB, one can use a magnet bar to separate the catalyst from solution easily. Artificial neural network (ANN) models can eliminate the huge part of experimental investigations in various filed of science and technology. After gathering some information about the methyl blue degradation, the ANN modeling was carried out to calculate the optimum values of initial variables to achieve the maximum removal efficiency. In this project, we used an initial ion concentration, the amount of nanocomposite that were used in photocatalyst activity and removal time as initial variables, finally the removal efficiency of pollution (MB) was considered as the output. In this project, we used a genetic algorithm (GA) to trained models and predation.

How to cite this article
Jarollahi S, Nabiyouni G, Sorinezami Z, Shabani A. Synthesis and Characterization of Fe_3O_4/TiO_2/Ag Magnetic Nanocomposite with Enhanced Photocatalytic Activity for Methylene Blue Degradation and Modeling by an Artificial Neural Network (ANN). J Nanostruct, 2023; 13(2):359-372. DOI: 10.22052/JNS.2023.02.005

* *Corresponding Author Email: Soori@uoz.ac.ir*

INTRODUCTION

One of the most significant part of the water pollution is propagation of the organic dyes. The different sources of pollution could be as: paper, painting, food, and textileindustries. These organic dyes, like methylene blue (MB), are hazardous to the environment and human life because of their substantial toxicity property. Therefore in the recent decades, scientists investigate their environmental effects and try to reduce them as much as they can. After a comprehensive study, two methods have been introduced to degrade organic dyes emissions, named as physical absorption and chemical methods. The physical adsorption has low efficiency and cannot be removed from organic dyes completely. However, some chemical methods indicate different results and lead to more effective removal of organic dyes compare with the physical absorption. These chemical methods can make non-toxic materials by changing the structure of organic dyes. [1-11]

Among many materials that could help humans to solve pollution issues and degenerate the organic dies, noble metals such as Ag, Au, Pt, and Cu have particular situations, because these metals show interesting property named SPR (Surface Plasmon Resonance). This phenomena happen when the frequency of conduction electrons in metals, be equal to the frequency of photon, emitted to the surface. In this situation, the free electrons in the metal surface oscillate with the frequency of the emitted photon. If the particle size of metal components decreases and tends to the nano size, one faced by LSPR (Local surface Plasmon Resonance) phenomena. This event appears in metallic nanoparticles. In fact, the strong interaction between the metallic nanoparticles and light takes place within a specific wavelength. By controlling the nanoparticlessize, one can change the interaction wavelength and optical properties of metal. One of the most interesting noble metals for researchers in recent decades, is Ag. Because of the high electrical, optical, and thermal conductivity of Ag, and also its lower price compare to Au and Pt, the interest in utilizing the Ag nanoparticles is ever growing. Silver nanoparticles are extraordinarily efficient at absorbing and scattering light and depend upon the size and shape of the particle. For example, by modifying the silver nanoparticles, the SPR wavelength peak can be tuned from 400 nm (violet light) to 530 nm (green light) [12-23].

The crystalline structure of Fe_3O_4 ferrite, is an inverse cubic spinel. In this formation, the iron ions are shared between tetrahedral and octahedral sites. The Fe^{3+} and Fe^{2+} ions occupied octahedral sites in the same ratio and tetrahedral sites being occupied just by Fe^{3+} ions. In fact, this dispersion of iron ions, create the tangible magnetic property of Fe_3O_4 ferrite. The magnetic interaction among octahedral ions shows ferromagnetic future and among iron ions at octahedral and tetrahedral sites is antiferromagnetic. Overall Fe_3O_4 shows ferri-magnetic behavior.

Especial properties of Fe_3O_4 attracted massive attention in several applications in recent years, including: magnetic hyperthermia and cancer treatment, smart drug delivery system and delivery drug to specific targets, biological separation mechanism, magnetic resonance imaging (MRI) technology, different wastewater treatment technique, heterogeneous catalysis, and various photocatalytic activities.Although balk Fe_3O_4 ferrite indicates ferri-magnetic property, but in the nanoparticle size, because of the superparamagnetic behavior, it is a good candidate for use in photocatalysis field. This future creates the ability to remove composite catalysts from the solution, easily by external magnetic field, because of to their excellent magnetic and dielectric properties.Also this future could play vital roles in numerous scientific and research branches such as new generation of bioelectrochemical sensors, biotechnology(biomedicine), development of new medical diagnosis, environmental remediation, catalysis, super-capacitors and lithium-ion batteries in electric vehicles and portable electronics, data storage, magnetic fluids as part of cooling systems, photocatalysis, microwave absorption covering equipment, carriers of drug or gene delivery, improve contrast agents for magnetic resonance imaging biomolecules separation, are some of the potential applications for Fe_3O_4 and its nanocomposites. [24-33]

On the other hand, Remarkable mechanical and optical properties and as well as their wide of utilities, lead to make the TiO_2 (N-type semiconductor) nanoparticles as one of the vital catalyst that attracted the attention in the recent years. Suitable difference between the valence and conduction bands (3.2 eV), Indirect band gap, non-toxic, low price of synthesis, and hydrophilic features are some advantages of using TiO_2.

TiO_2 nanoparticles observe in four kinds of

structures: Anatase, Rutile, Brookite, and Beta. Behind all advantages of these nanoparticles, there are some the limitations as well. For example, for high photocatalytic activity, the band gap permits only ultraviolet(UV) visible spectrum to be proficiently used.

One should notice that only less than 5% of sunlight contains UV spectrum and if one wants to use it, there would be a colossal problem.

Recent reports reveal the new generation of nanocomposites that show the magnetic and optical properties at same time and shape bright future in field of material science and modern technology. The large number of employment exhibited by the magnetic-plasmonic-semiconductor materials. These applications get into multiples acknowledgment areas, such as biology, catalysis, biomedicine, and optoelectronics. Generally, the magnetic-plasmonic-semiconductor materials are composed of three parts. The family of ferrites as in their magnetic part of, noble metals such as Au, Ag, Cu, or Pt as plasmonic part, and finally special metal oxide as semiconductor parts such as titanium dioxide.Depend on the final goal and usages, we can determine to factors that have huge effect on functionality of the magnetic-plasmonic-semiconductor materials, particle's size and shape. In this structure, noble metals have two various applications. First they react as part of degrade organic dyes individually, and the second, is help the semiconductor materials such as TiO_2 nanoparticles to increase the hole-electron combination time [34-40]. Also some papers published and mentioned to Eco-friendly way to synthesis nanocomposite to degradation of various organic and non-organic pollutions. For example using different juices as green fuel or organic surfactant as new way to control the nanocomposite size. These researches show the high value of this issue for earth and future of human life.

Artificial intelligence (AI) is the new branch of computer science that mention to abilities of simulation of human brain processes by machines. This technology is programmed to think and act like humans and their actions. For example, design special methods that due to the machines that exhibit features like related human mind, such as problem-solving or learning.The idea of creating artificial intelligence was designed special system that thinking and reacting like human being to find the best way to achieve a specific targets. One of the main part of artificial intelligence is machine learning.This subset refers to thisconcept that computer programs can learn and adapt to new data without assistance of human and running automatically. Deep learning is the name of popular branch of machine learning that enable this automatic learning. These techniques work with absorbing theunstructured data from different sources, such as texts, images or videos.

Artificial neural network (ANN) is one of the subsets of deep learning computing tools that inspired the biological nervous network of human brains. The main target of ANN is to predict uncertain relationships between input and output parameters in a complicated system by the learning process. The researcher defined three various methods of learning, named: supervised, semi-supervised or unsupervised. An ANN contains nodes, and these processing units are made up of input and output units. In the supervised technique, the algorithm use data to recognize patterns by calculating the weights for each node. Although the neural network utilizes in recent years, but it has the enormous effects on exciting problems in different areas of science, medicine, and engineering, and cause incredible progress. Recently, ANN was employed in nano science and determined the relation between other measurement parameters that affect results. One of the interesting topics, in this case, is forecast the removal ofazo dyes in aqueous solutions. Finding optimized conditions to degenerate pollution could save time and eliminate expensive experimental research. [40-49]

In this paper, Fe_3O_4/TiO_2/Ag nanocomposite prepared for the effective catalytic degradation of methylene blue schematically is shown in Fig. 1. At first, Fe_3O_4 nanoparticles was synthesized by co-precipitation method. Then TiO_2 nanoparticles was coated to the Fe_3O_4surface, so that Fe_3O_4/TiO_2 nanocomposite was formed. In the next step, Ag nanoparticles was added and created a new layer on the surface Fe_3O_4/TiO_2. Therefore, Fe_3O_4/TiO_2/Ag magnetic nanocompositewas produced in three phases. Then the photocatalyst (in form of solid) was added to the aqueous solution of azo dyes (methylene blue) and the solution is put under the UV light to start degradation process. The product then was investigated for photocatalytic reduction of MB by monitoring a UV-visible spectrophotometer. Because of the magnetic property of nanocomposite, the photocatalyst

can be collecting from solution simply by using a magnet bar. The experiment is repeated and 20 points of experimental data with various initial ion concentrations, removal time and, adsorbent dosage parameters were collected, and the artificial neural network is employed to predict removal percentage.

MATERIALS AND METHODS

Materials

Iron(III) chloride ($FeCl_3.6H_2O$), Iron(II) chloride ($FeCl_2.4H_2O$), Silver nitrate ($AgNO_3$), sodium hydroxide (NaOH), methylene blue ($C_{16}H_{18}N3_sCl$), titanium (IV)isopropoxide (TIPP) (97 % purity) were purchased from Merck Company.

Synthesis magnetic nanocomposite Fe_3O_4/TiO_2/Ag

5.84g of $FeCl_3.6H_2O$ was dissolved in 200ml of distilled water and the solution was stirred using a magnet bar. After 5 min of mixing,2.16g of $FeCl_2.4H_2O$ was added to the solution. Meanwhile, the solution temperature increases. Afterward, added drop-wise NaOH (2M) was added into the solution until the solution color turned from yellow to black and the solution pH reaches to 10. After 1 h, the magnetic Fe_3O_4 nanoparticles were produced. At the next step, to synthesize the Fe_3O_4/TiO_2 nanocomposite, 2ml TIPP was injected to solution and was shaken for 2h, and followed by the sonication process which taken place for 1 h. At the final part of the synthesis, 1.2g of $AgNO_3$ dissolved in distilled water and was added to product to make Fe_3O_4/TiO_2/Ag nanocomposite. The sodium hydroxide was added to increase pH solution to 10. After using 50 min of ultrasonic process, the solution was mixed for 1 h by starrier. Finally, the solution was washed with distilled water 2 times and dried at 40 °C in an oven.

Degradation process of Azo dyes

To determine the effectiveness of Fe_3O_4/TiO_2/Ag nanocomposite to remove azo dyes from the solution, 0.5g of this nanocomposite was added to 200 ml of the dye solution (20 ppm). The solution was mixed and shaken by a mechanical stirrer for 1.5 h in dark environment to distinguishbetween the rate of adsorption and photocatalystefficiency. Next, the solution was transferred to a reactor with four 100 W UV lamps. The solution was stirred for 1 h while it was under the irradiation of UV light. Finally, the nanocompositewas separated from the solution by a magnet bar. The solutionwas filtered, centrifuged, and their concentration was analyzed to determine the methyl blue concentration.

Characterization

The phase characterization and XRD patterns, were recorded by a Philips, X-ray diffractometer using Ni-filtered Cu K_a radiation. For ultrasonic irradiation, we have used a multi-wave ultrasonic generator (FAPN) with oscillation frequency of 20 kHz, and maximum power of 150 W. SEM images

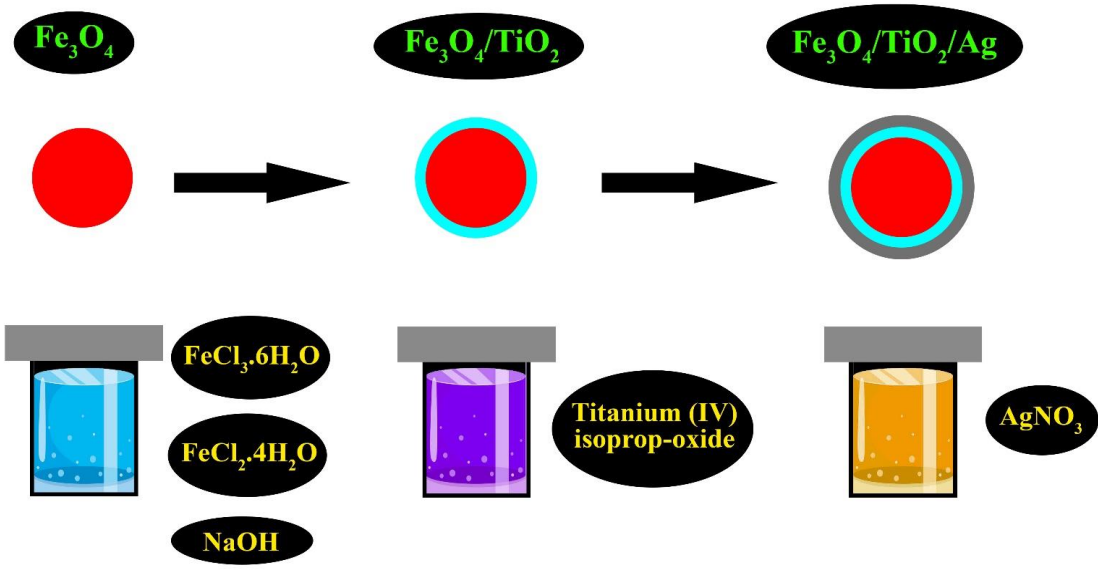

Fig. 1. Schematic of preparation Fe_3O_4/TiO_2/Ag magnetic nanocomposite

were taken using aMIRA3 TESCAN instrumen. The samples were coated by a very thin layer of platinumto prevent the charge accumulation and gain a high resolution and better contrast. To investigate the magnetic property of samples and analyze the hysteresis loop, we were employed an alternating gradient force magnetometer (AGFM) made by MeghnatisDaghighKavir. In order to check the chemical bonds of the compositions and purity percentage of the samples, Fourier transform infrared spectrometer (FT-IR) made by BRUKER (ALPHA) was employed.To calculate the concentration of initial and final methyl blue solution, an UV-Vis spectrophotometer (SCO) was used.

Artificial neural network

We used the Tensor Flow platform to create and learn algorithms. To design the experiments, initial ion concentration, removal time, and adsorbent dosage were selected as input variables, and the removal percentage of methyl blue was chosen as the output. The network architect consists of three nodes as input, hidden layer, and one node as output. The input neurons relate to the node j in the hidden layer by

$$\partial_j = \sum_{i=1}^{h} (X_i W_{ij}) + \theta_j \quad (1)$$

Also the output from j the neuron of the hidden layer is given by

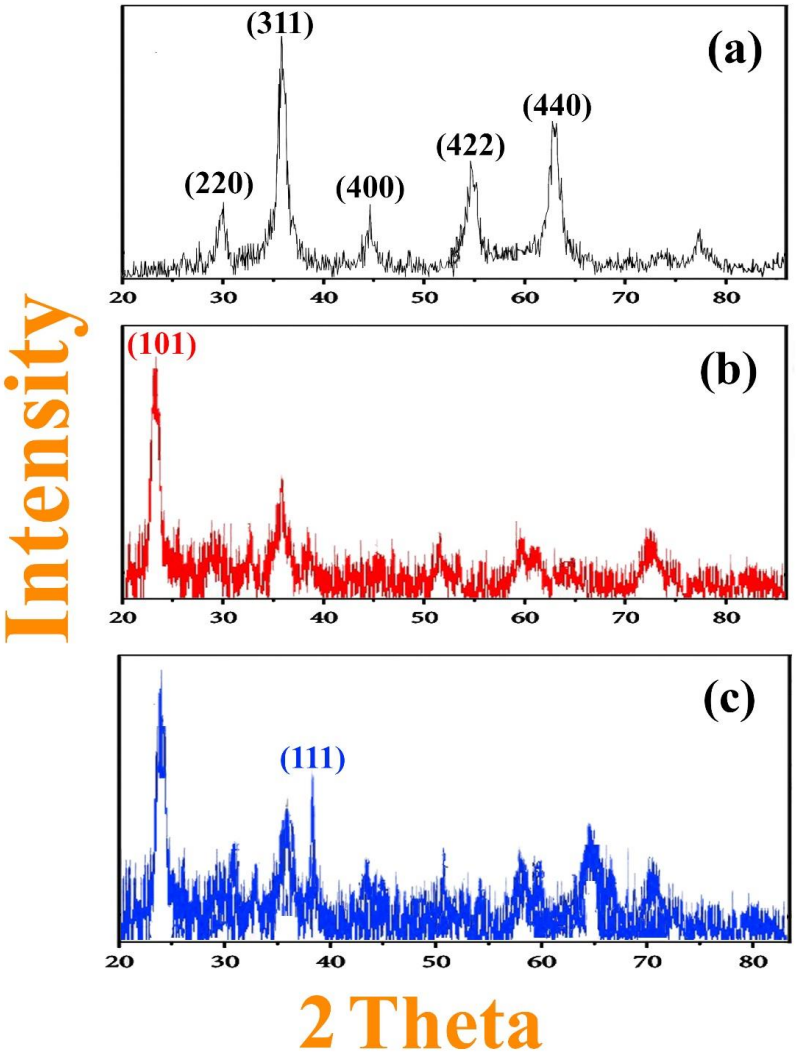

Fig. 2. XRD patterns of the prepared materials, (a) Fe_3O_4 (b) Fe_3O_4/TiO_2 (c) Fe_3O_4/TiO_2/Ag

$$O_j = f(\partial_j) \quad (2)$$

In the above equations, h is the number of nodes in the input layer, t is the number of neurons in the hidden layer, θ_j is the bias term, W is the weighting factor, and f is the activation function of the hidden layer. In the end of ANN structure, the output of the kth neuron in the output layer is given by:

$$Y_k = \sum_{i=1}^{h}(O_i W_{ik}) + b_k \qquad k = 1, 2, ..., n \quad (3)$$

Where W is the weighting factor, b_k is the bias term, and n is the number of neurons in the output layer.

The experimental points were divided into two categories. First one, consists of 15 points to train the model and 5 points to test. We were used root mean square error (RMSE) as model to prediction, and to compile the model the binary cross-entropy was applied as loss function, and Adam as optimizer.

RESULTS AND DISCUSSION

Figs. 2(a-c) show the XRD pattern for Fe_3O_4 (a) nanoparticles, (b) Fe_3O_4/TiO_2 and (c) Fe_3O_4/TiO_2/Ag nanocomposite. The main crystallographic planes of Fe_3O_4 are (220), (311), (400), (422), and (440) planes. The low intensity of background shows the high purity of the sample, and the pattern is indexed as a cubic phase with JCPDS of 03-0863 reference card. The Fe_3O_4/TiO_2XRD pattern shows an additional peak related to the TiO_2 nanoparticles. The sharpest peak with the highest intensity is due to the (101) plate. Adding the Ag nanoparticle to the composite, leads to a decrease of peak intensities because of forming the multiphase structure. The (111) peak in Fig. 2(c), relates to Ag nanoparticles. The crystalline sizes of samples were calculated by the Scherrer equation ($D_c = K\lambda/\beta Cos\Theta$) (4), where, D_c is the crystalline size, K is so-called shape factor taking equal to 0.9, λ is the X-ray wavelength. All samples have crystalline sizes less than 20nm.

Figs. 3(a-f) shows the morphology of Fe_3O_4 nanoparticles which synthesized at different temperatures. The nanoparticle shapes are mostly spherical with a reasonably high level of purity and average diameter of less than 60nm. Synthesize at high temperatures leads to decrease in the nanoparticles sizes, because temperature has many effects on nucleation growth. On the other hand, nanoparticles grown a lower temperatures are more uniform and have larger sizes. However, we observed that the reaction rate increases with

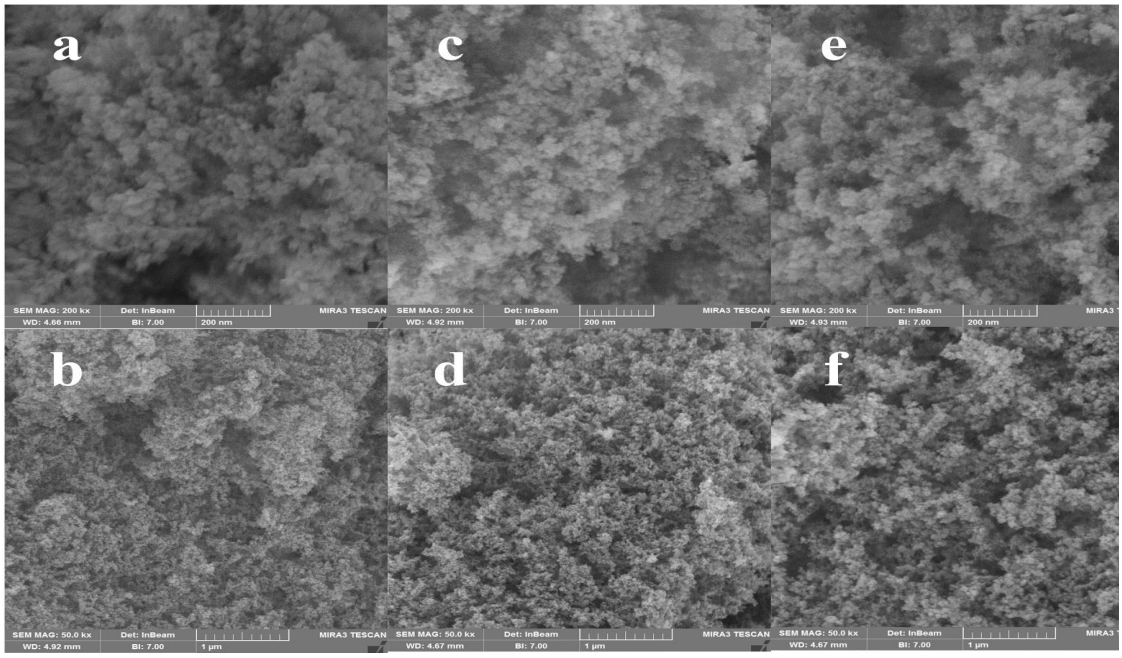

Fig. 3. SEM images of Fe_3O_4 nanoparticles in different magnificationsat different temperature. (a,b) 30^O C (c,d) 60^O C (e,f) 90^O C

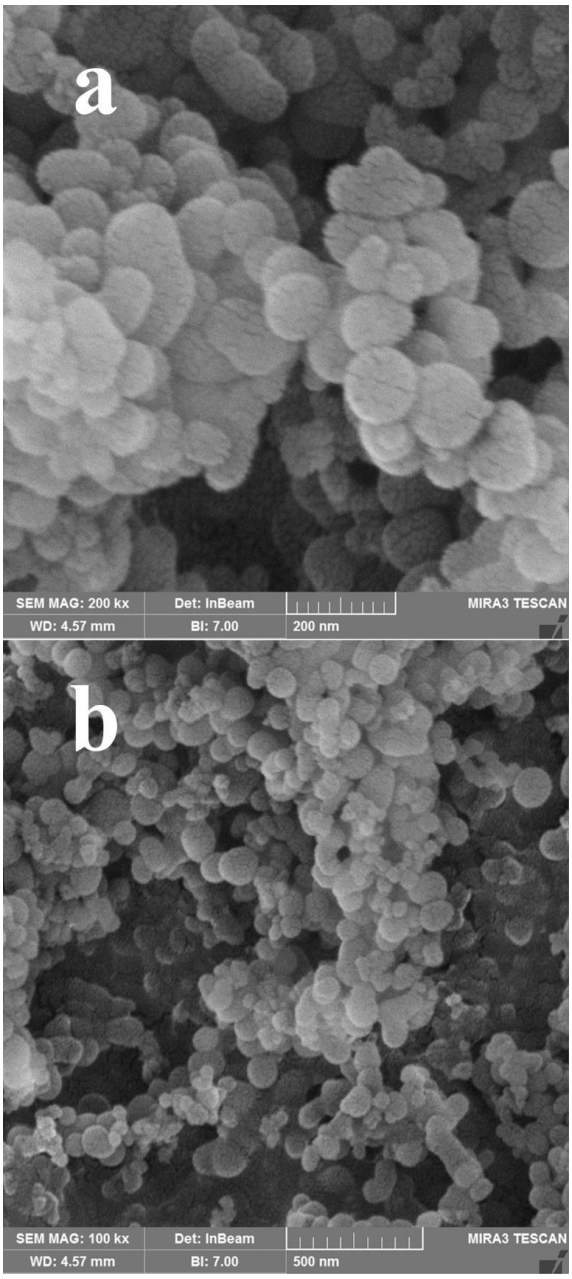

Fig. 4. SEM images of Fe_3O_4/TiO_2 nanocomposite in different magnifications

increasing the reactive temperature.

Figs. 4(a-b) shows the SEM images of Fe_3O_4/TiO_2 nanocomposites and confirm that the spherical nanocomposites were successfully synthesized. The TiO_2 nanoparticles had enough time to load on the Fe_3O_4 nanoparticlessurfaces, and the sonication process helped to achieve high purity of nanocomposite.

The morphology of Fe_3O_4/TiO_2/Ag nanocomposite illustrates in Figs. 5(a-b) with different magnification. The average size of the synthesized nanocomposite was determined under 70 nm. One reason for this result could be as: gradually increasing of the pH solution gives enough time to bond Fe_3O_4/TiO_2. Also, the sonication leads to prevent the clumping

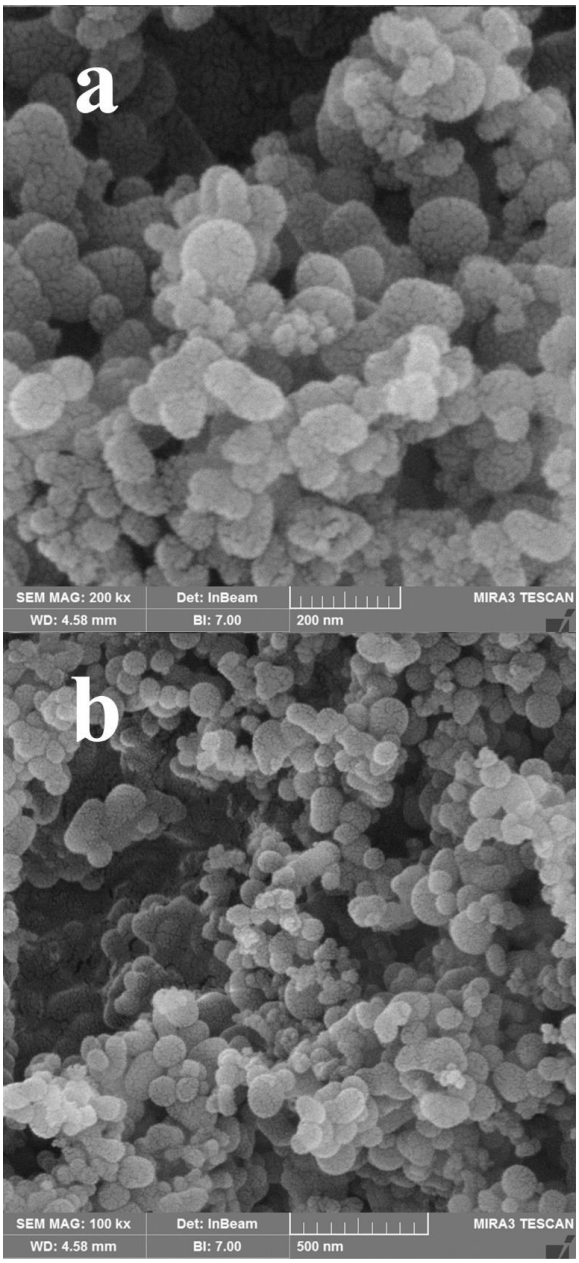

Fig. 5. SEM images of Fe_3O_4/TiO_2/Agnanocomposite in different magnifications

of nanocomposites. The spherical shape of nanocomposites indicate that the Fe_3O_4/TiO_2/Agmagnetic nanocomposites are suitable candidate to usage in photocatalytic activities because the high rate of effective surface in this morphology due to more chemical reactions.

Fig. 6 exhibits the FT–IR spectrum of theFe_3O_4 nanoparticles, Fe_3O_4/TiO_2andFe_3O_4/TiO_2/Ag nanocomposite. The peak at around 3419 cm^{-1} corresponds to the stretching mode of OH group adsorbed on the surface of the nanoparticles and the peak at 1640 cm^{-1} corresponds to the bending vibration of H_2O. The peaks at 450 and 583 cm^{-1} correspond to the Fe–O bonds. The peak at 781 cm^{-1} which attributes to the Ti–O bond in TiO_2 shows the metal-oxygen bond.

The magnetic property of Fe_3O_4 nanoparticles, Fe_3O_4/TiO_2, and Fe_3O_4/TiO_2/Ag nanocomposites

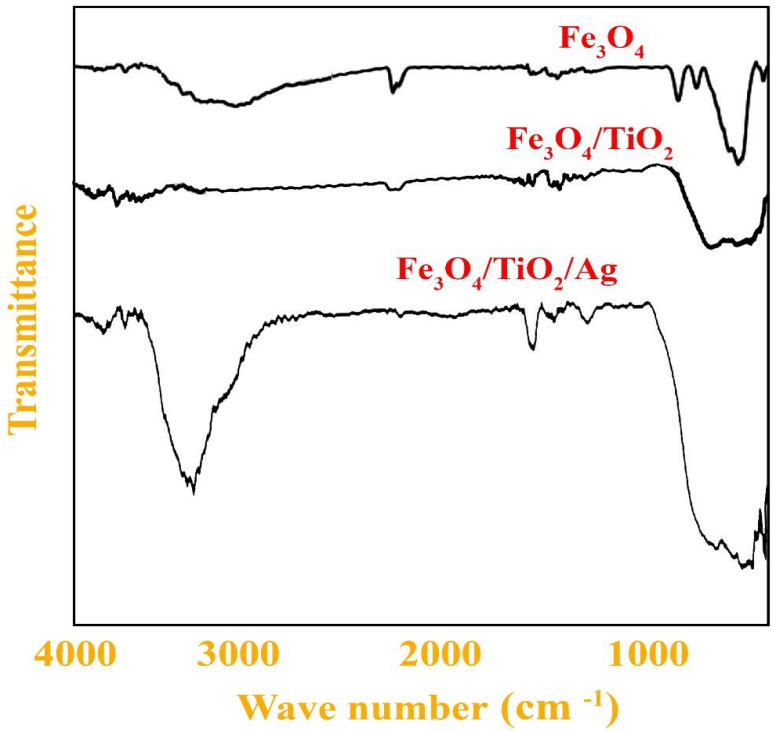

Fig. 6. FT–IR spectrum ofFe_3O_4 nanoparticles, Fe_3O_4/TiO_2 and Fe_3O_4/TiO_2/Ag nanocomposite

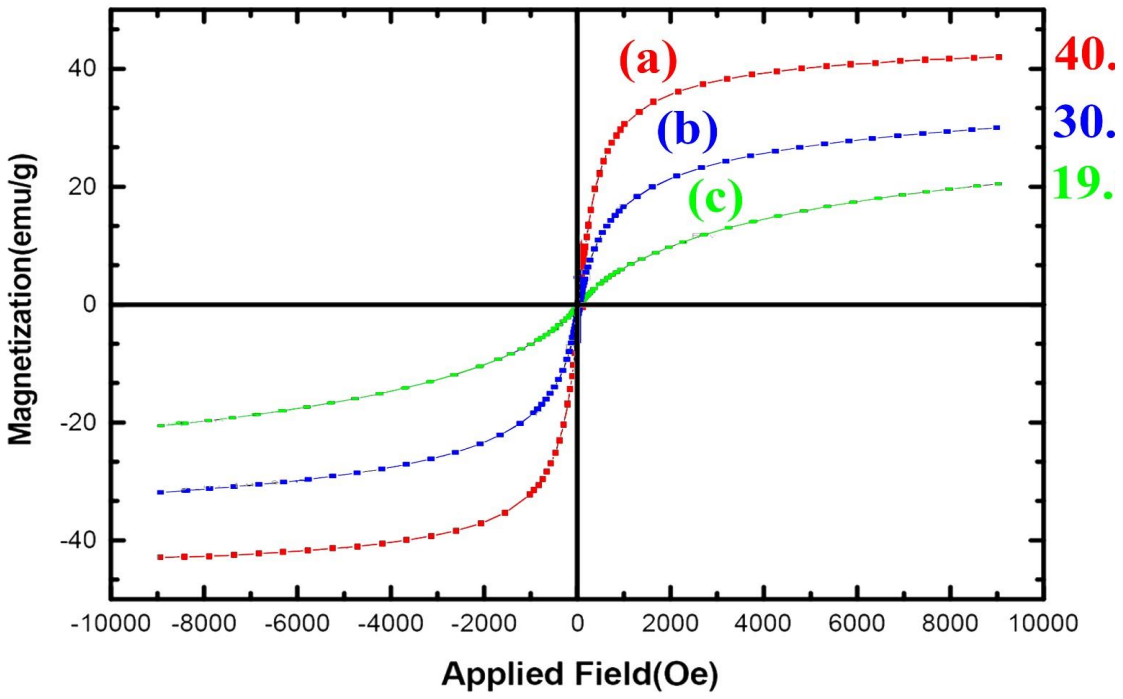

Fig. 7. Hysteresis loops for: (a) Fe_3O_4 nanoparticles, (b) Fe_3O_4/TiO_2, (c) Fe_3O_4/TiO_2/Ag nanocomposites

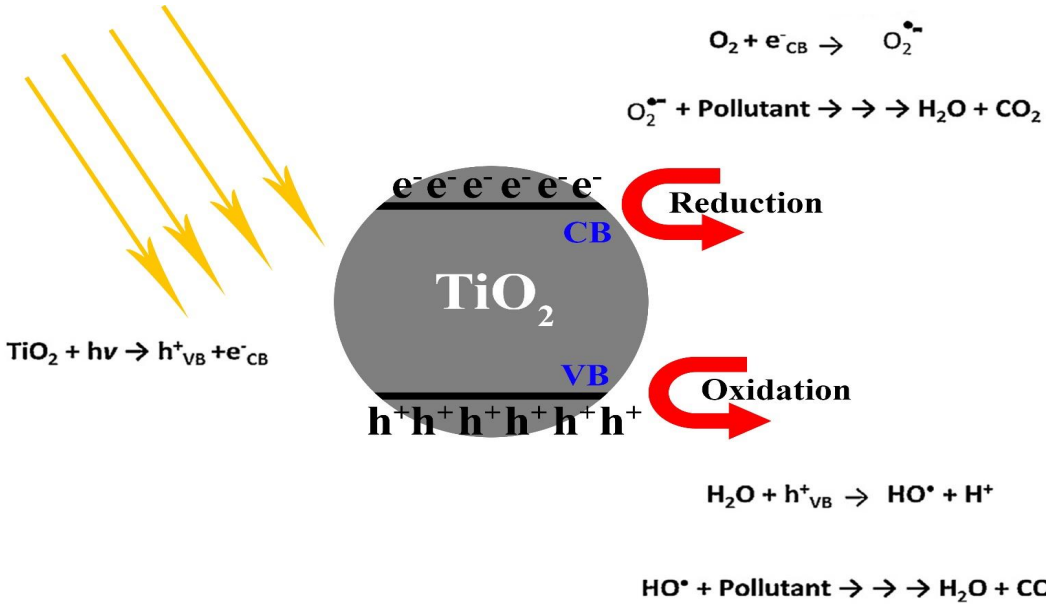

Fig. 8. Schematic of degradation mechanism of organic dyes under UV irradiation by TiO_2 nanoparticles

were investigated and the results are illustrated in Figs. 7(a-c). The hysteresis loop for Fe_3O_4 nanoparticlesreveals the superparamagnetic behavior with the magnetic saturation around 40 emu. By introducing TiO_2nanoparticles and producing Fe_3O_4/TiO_2, magnetic saturation of Fe_3O_4 decreases, because the appearance of TiO_2 nanoparticles in composite, covers the Fe_3O_4 nanoparticles, the fact that confirmed by the hysteresis loop of Fe_3O_4/TiO_2 nanocomposite at Fig. 7(b). Same effect is happen when the magnetic property and hysteresis loop of Fe_3O_4/TiO_2/Ag nanocomposite was studied at Fig. 7(C).

The Fe_3O_4/TiO_2/Ag nanocomposites degrademethyl blue in two methods. In the first method TiO_2 nanoparticles act as a semiconductor. The schematic diagram for this process is shown in Fig. 8. The emitted photons affect the electron from the valance band and transfer them to the conduction band. Therefore there are some electrons in the conduction band and some holes in the valance band. The electrons react with oxygen in the air, and superoxide anion is created. Because of the reaction of waterand holes in the valance band, hydroxyl radicals are appeared. $.O_2^-$ and .OH radicals degradeof azo dyes and other pollutions in aqueous solution. The second phenomena that help to remove pollutions is by the effect of the Ag nanoparticles and LSPR property. Since the radiation photons to the surface of silver nanoparticles and the LSPR effect, the electrons start to oscillate with a frequency equals to resonance frequencyof Ag nanoparticles (Fig. 9). In this case, the LSPR effect creates positive

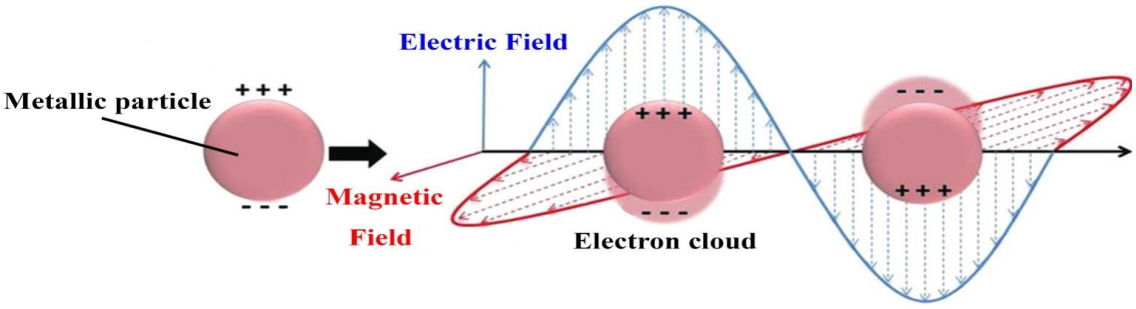

Fig. 9. Schematic of LSPR effect of Ag nanoparticles

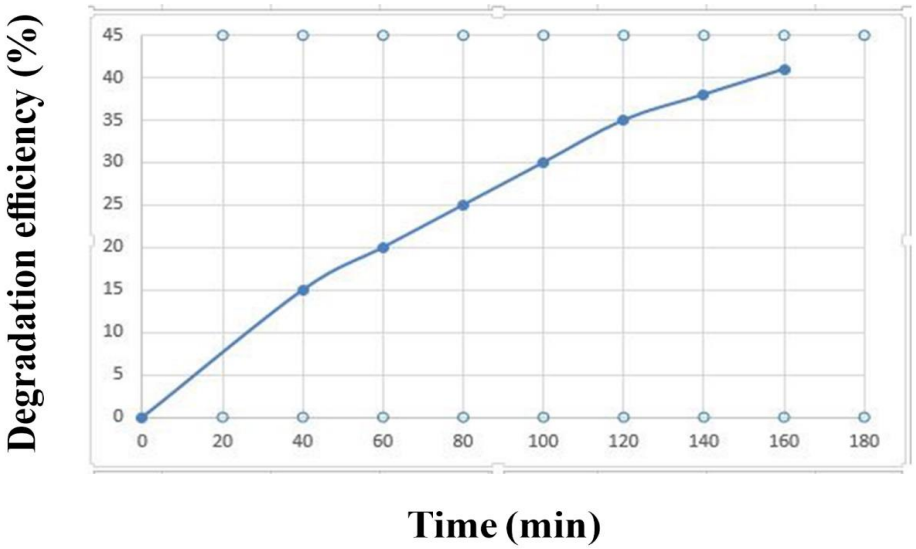

Fig. 10. Photocatalytic degradation of methylene blue at different times against UV light

and negative charges and enters into removing dyes pollution. Fig. 10 indicates photocatalytic degradation efficiency at different times against UV spectrum (using the 0.5gr of $Fe_3O_4/TiO_2/Ag$). To calculate the degradation efficiency, the following equation was used:

$$\frac{C_0 - C}{C_0} \times 100 \quad (4)$$

Where, the C_0 is the initial concentration of the solution, and C is the final concentration after the photocatalyst process.

Table 1. Experimental data set design, including 20 different samples

Sample Number	Adsorbent dosage (g)	Initial ion concentration (mg/L)	Removal time (min)	Removal percentage (%)
1	1.05	100	100	65.23
2	1.04	100	90	60.54
3	1.08	120	70	61.21
4	1.11	120	40	70.58
5	1.06	140	90	72.54
6	1.07	100	80	67.84
7	1.04	120	85	65.24
8	1.09	130	70	68.59
9	1.08	100	60	70.21
10	1.05	140	100	69.74
11	1.06	90	95	68.65
12	1.05	110	110	65.03
13	1.08	120	100	68.27
14	1.11	120	60	73.28
15	1.07	140	85	74.14
16	1.06	130	95	66.39
17	1.06	120	90	68.43
18	1.09	100	70	69.19
19	1.1	110	60	68.34
20	1.05	130	100	70.28

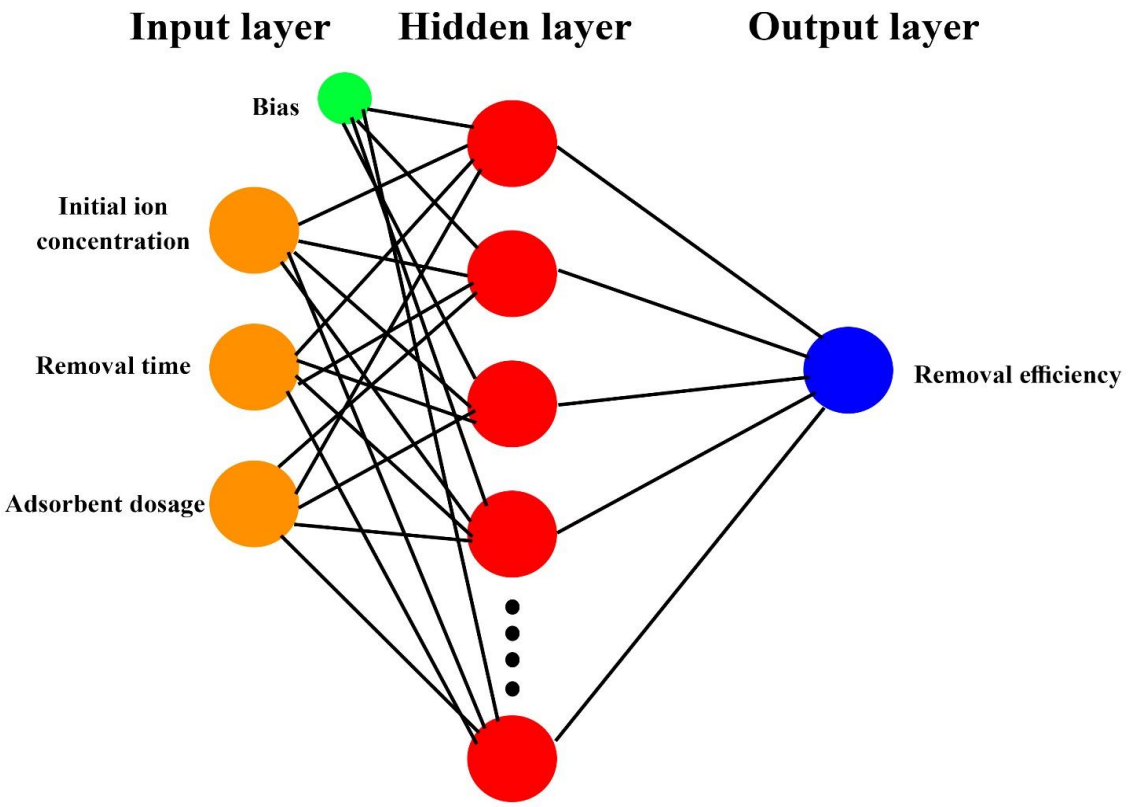

Fig. 11. Schematic of ANN architected

Table 2.Experimental and prediction values of degradation percentage of methyl blue

Sample Number	Experimental Removal percentage (%)	Predictional Removal percentage (%)
2	60.54	61.12
7	65.24	66.32
13	68.27	67.57
17	68.43	69.51
19	68.34	69.47

The dataset shown in the Table 1 contain 20 different experimental date (called samples) that were measured in different situations. They were randomly divided into two sets, which were used for training and testing the model. The training group includes 15, and the test branch has 5 samples. The training data were used to estimate and calculate the parameters of the ANN algorithm and the testing data was applied to show that the network parameters are valid. This network has 3 layers called: input, hidden, and output. In this research, the ANN network has 3 parameters as input, including: initial ion concentration, removal time and adsorbent dosage. The schematic of ANN architected is shows in Fig. 11. All of the input and output values were normalized in the range of 0 and 1. One of the critical point to design the algorithm is setting and finding optimized activated function, loss function, and also choosing the optimum number of nodes in the hidden layer. Regarding the above mentioned concepts, the ANN network introduce the best results just by examine and use the experience of AI researchers in different fields. The difference between experimental and

prediction values of degradation percentage of methyl blue are compared and the results is summarized in Table 2. The rate of predicted accuracy is acceptable despite the number of samples is limited. To achieve more accuracy, one need more samples and more power of algorithm by taking more hidden layers and input nodes into account. Based on the obtained results, by controlling the input parameters, it is possible to estimate the removal percentage and use them in industrial activities.

CONCLUSION

In this paper, we have synthesized Fe_3O_4/TiO_2/Ag magnetic nanocomposite and use two different structures (metal oxide and metal) to degrademethyl blue. The chemical properties and constituent of this Fe3O4/TiO_2/Ag catalyst were characterized by the SEM, TEM, EDS, FT-IR, XRD and VSM methodsThe LSPR effect of Ag nanocomposite and also semiconductor property of TiO_2 nanocomposite at the same time help to record better efficiency of degradation, compared with the structures of Ag, TiO_2, andFe_3O_4, individually. Finally, by collecting the information about the samples and preparing a dataset of parameters, we used the ANN method to predict the removal percentage of methyl blue. Our model consists of 3 layers, i.e. input, hidden and output layers. Three parameters of initial ion concentration, removal time, and adsorbent dosage were chosen as input variables. Also, the removal percentage of methyl blue was selected as the output. In spite of having some limitations such as the finite input parameters and the number of samples, the accuracy of prediction is quite acceptable, indicating the right way and that the ANN algorithm is a powerful technique. Therefore we could use ANN as new way to remove huge expensive experimental costs and also increase the accuracy of empirical conclusions. We should notice that access to more datasets in various fields could help us to achieve these targets easily and immediately.

CONFLICT OF INTEREST

The authors declare that there is no conflict of interests regarding the publication of this manuscript.

REFERENCES

1. Shabani A, Nabiyouni G, Ghanbari D. Preparation and photocatalytic study of $CoFe_2O_4/TiO_2$/Au nanocomposites and their applications in organic pollutant degradation and modeling by an artificial neural network (ANN). Journal of Materials Science: Materials in Electronics. 2022;33(13):9885-9904.
2. Kumavat SR, Mishra S. Green Synthesis of Silver Nanoparticles Using Novel Launaea Procumbens Leaves Extract and Screening Its Antibacterial Activity. Research Square Platform LLC; 2021.
3. Masoumi S, Nabiyouni G, Ghanbari D. Photo-degradation of azo dyes: photo catalyst and magnetic investigation of $CuFe_2O_4$–TiO_2 nanoparticles and nanocomposites. Journal of Materials Science: Materials in Electronics. 2016;27(9):9962-9975.
4. (GaIn)(NAsSb): The Challenges for Long Wavelength Communications Devices. Compound Semiconductors 2004: CRC Press; 2005. p. 95-104.
5. Mukai SR. Preface: Eighth Pacific Basin Conference on Adsorption Science and Technology. Adsorption. 2019;25(6):1033-1034.
6. Rafatullah M, Sulaiman O, Hashim R, Ahmad A. Adsorption of methylene blue on low-cost adsorbents: A review. J Hazard Mater. 2010;177(1-3):70-80.
7. Crini G. Non-conventional low-cost adsorbents for dye removal: A review. Bioresour Technol. 2006;97(9):1061-1085.
8. Gupta VK, Suhas. Application of low-cost adsorbents for dye removal – A review. J Environ Manage. 2009;90(8):2313-2342.
9. Sanghi R, Verma P. Decolorisation of aqueous dye solutions by low-cost adsorbents: a review. Coloration Technology. 2013;129(2):85-108.
10. Woo MA, Woo Kim T, Paek M-J, Ha H-W, Choy J-H, Hwang S-J. Phosphate-intercalated Ca–Fe-layered double hydroxides: Crystal structure, bonding character, and release kinetics of phosphate. J Solid State Chem. 2011;184(1):171-176.
11. Wang L, Xu X, Evans DG, Duan X, Li D. Synthesis and selective IR absorption properties of iminodiacetic-acid intercalated MgAl-layered double hydroxide. J Solid State Chem. 2010;183(5):1114-1119.
12. Baliarsingh N, Parida KM, Pradhan GC. Influence of the nature and concentration of precursor metal ions in the brucite layer of LDHs for phosphate adsorption – a review. RSC Advances. 2013;3(46):23865.
13. Yang S, Zhang S, Wang H, Yu H, Fang Y, Peng F. Controlled preparation of Ag–Cu_2O nanocorncobs and their enhanced photocatalytic activity under visible light. Mater Res Bull. 2015;70:296-302.
14. Jian L, Cai D, Su G, Lin D, Lin M, Li J, et al. The accelerating effect of silver ion on the degradation of methyl orange in Cu_2O system. Applied Catalysis A: General. 2016;512:74-84.
15. Meir N, Jen-La Plante I, Flomin K, Chockler E, Moshofsky B, Diab M, et al. Studying the chemical, optical and catalytic properties of noble metal (Pt, Pd, Ag, Au)–Cu_2O core–shell nanostructures grown via a general approach. J Mater Chem A. 2013;1(5):1763-1769.
16. Kuo C-H, Hua T-E, Huang MH. Au Nanocrystal-Directed Growth of Au–Cu_2O Core–Shell Heterostructures with Precise Morphological Control. Journal of the American Chemical Society. 2009;131(49):17871-17878.
17. Zhang L, Blom DA, Wang H. Au–Cu_2O Core–Shell Nanoparticles: A Hybrid Metal-Semiconductor Heteronanostructure with Geometrically Tunable Optical Properties. Chem Mater. 2011;23(20):4587-4598.
18. Liu D-Y, Ding S-Y, Lin H-X, Liu B-J, Ye Z-Z, Fan F-R, et al. Distinctive

Enhanced and Tunable Plasmon Resonant Absorption from Controllable Au@Cu_2O Nanoparticles: Experimental and Theoretical Modeling. The Journal of Physical Chemistry C. 2012;116(7):4477-4483.
19. Westcott SL, Jackson JB, Radloff C, Halas NJ. Relative contributions to the plasmon line shape of metal nanoshells. Physical Review B. 2002;66(15).
20. Kong L, Chen W, Ma D, Yang Y, Liu S, Huang S. Size control of Au@Cu_2O octahedra for excellent photocatalytic performance. J Mater Chem. 2012;22(2):719-724.
21. Lu B, Liu A, Wu H, Shen Q, Zhao T, Wang J. Hollow Au–Cu_2O Core–Shell Nanoparticles with Geometry-Dependent Optical Properties as Efficient Plasmonic Photocatalysts under Visible Light. Langmuir. 2016;32(12):3085-3094.
22. Height MJ, Pratsinis SE, Mekasuwandumrong O, Praserthdam P. Ag-ZnO catalysts for UV-photodegradation of methylene blue. Applied Catalysis B: Environmental. 2006;63(3-4):305-312.
23. Wang L, Sun Y, Wang J, Wang J, Yu A, Zhang H, et al. Preparation of surface plasmon resonance biosensor based on magnetic core/shell Fe_3O_4/SiO_2 and Fe_3O_4/Ag/SiO_2 nanoparticles. Colloids Surf B Biointerfaces. 2011;84(2):484-490.
24. Zhang Z, Wang Y, Qi Z, Zhang W, Qin J, Frenzel J. Generalized Fabrication of Nanoporous Metals (Au, Pd, Pt, Ag, and Cu) through Chemical Dealloying. The Journal of Physical Chemistry C. 2009;113(29):12629-12636.
25. Morel A-L, Nikitenko SI, Gionnet K, Wattiaux A, Lai-Kee-Him J, Labrugere C, et al. Sonochemical Approach to the Synthesis of Fe_3O_4@SiO_2 Core−Shell Nanoparticles with Tunable Properties. ACS Nano. 2008;2(5):847-856.
26. Behzadi M, Jarollahi S, Ahsani Irvani M, Ghanbari D, Green Synthesis and Antibacterial Activity of Silver Nanoparticles Using Dracocephalum Moldavica Leaves Extract, Journal of Nanostructures 2022; 12 (4): 1059-1066.
27. Jia S, Song T, Zhao B, Zhai Q, Gao Y. Regular Fe_3O_4 octahedrons with excellent soft magnetic properties prepared by dealloying technique. J Alloys Compd. 2014;585:580-586.
28. Yuan Y, Chen S, Paunesku T, Gleber SC, Liu WC, Doty CB, et al. Epidermal Growth Factor Receptor Targeted Nuclear Delivery and High-Resolution Whole Cell X-ray Imaging of Fe_3O_4@TiO_2 Nanoparticles in Cancer Cells. ACS Nano. 2013;7(12):10502-10517.
29. Crossley EL, Aitken JB, Vogt S, Harris HH, Rendina LM. Selective Aggregation of a Platinum–Gadolinium Complex Within a Tumor-Cell Nucleus. Angew Chem Int Ed. 2010;49(7):1231-1233.
30. Lu AH, Salabas EL, Schüth F. Magnetic Nanoparticles: Synthesis, Protection, Functionalization, and Application. Angew Chem Int Ed. 2007;46(8):1222-1244.
31. Yavuz CT, Mayo JT, Yu WW, Prakash A, Falkner JC, Yean S, et al. Low-Field Magnetic Separation of Monodisperse Fe_3O_4 Nanocrystals. Science. 2006;314(5801):964-967.
32. Shen YF, Tang J, Nie ZH, Wang YD, Ren Y, Zuo L. Preparation and application of magnetic Fe_3O_4 nanoparticles for wastewater purification. Sep Purif Technol. 2009;68(3):312-319.
33. Ramezani S, Mashhadizadeh M H, Jahani R , Kamali M. Carbon nanotube grafted pyridinuim compound as a neutral ion-carrier of carbon paste electrode for sub-nanomolar simultaneous monitoring of Cu (II) and Hg (II). International Journal of Environmental Analytical Chemistry, 2023; DOI: 10.1080/03067319.2023.2249826.
34. Shabani A, Nabiyouni G, Saffari J, Ghanbari D. Photo-catalyst Fe_3O_4/TiO_2 nanocomposites: green synthesis and investigation of magnetic nanoparticles coated on cotton. Journal of Materials Science: Materials in Electronics. 2016;27(8):8661-8669.
35. Lee S, Byun K, Park J, Kim S, Lee J, Chang S, et al. Homogeneous ZnS coating onto TiO_2 nanoparticles by a simple one pot sonochemical method. Chem Eng J. 2008;139(1):194-197.
36. Narayani H, Arayapurath H, Shukla S. Using Fenton-Reaction as a Novel Approach to Enhance the Photocatalytic Activity of TiO_2-γ-Fe_2O_3 Magnetic Photocatalyst Undergoing Photo-Dissolution Process without Silica Interlayer. Catal Lett. 2013;143(8):807-816.
37. He Q, Zhang Z, Xiong J, Xiong Y, Xiao H. A novel biomaterial — Fe_3O_4:TiO_2 core-shell nano particle with magnetic performance and high visible light photocatalytic activity. Opt Mater. 2008;31(2):380-384.
38. Behnia B, Anvari AA, Safardoust-Hojaghan H, Salavati-Niasari M. Positive effects of novel nano-zirconia on flexural and compressive strength of Portland cement paste. Polyhedron. 2020;177:114317..
39. Amini R, Nabiyouni G, Jarollahi S. Removal of azo dyes pollutants: Photo catalyst and magnetic investigation of iron oxide-zinc sulfide nanocomposites. Journal of Nanostructures. 2021; 11 (1): 95-104.
40. Ruíz-Baltazar ÁdJ. Green synthesis assisted by sonochemical activation of Fe_3O_4-Ag nano-alloys: Structural characterization and studies of sorption of cationic dyes. Inorg Chem Commun. 2020;120:108148.
41. Zhao S, Talasila M, Jacobson G, Borcea C, Aftab SA, Murray JF. Packaging and Sharing Machine Learning Models via the Acumos AI Open Platform. 2018 17th IEEE International Conference on Machine Learning and Applications (ICMLA); 2018/12: IEEE; 2018.
42. Saracoglu Ö. An Artificial Neural Network Approach for the Prediction of Absorption Measurements of an Evanescent Field Fiber Sensor. Sensors. 2008;8(3):1585-1594.
43. Hagan MT, Menhaj MB. Training feedforward networks with the Marquardt algorithm. IEEE Trans Neural Networks. 1994;5(6):989-993.
44. Saini LM, Soni MK. Artificial neural network based peak load forecasting using Levenberg–Marquardt and quasi-Newton methods. IEE Proceedings - Generation, Transmission and Distribution. 2002;149(5):578.
45. Bekat T, Erdogan M, Inal F, Genc A. Prediction of the bottom ash formed in a coal-fired power plant using artificial neural networks. Energy. 2012;45(1):882-887.
46. Sadeghiamirshahidi M, Eslam kish T, Doulati Ardejani F. Application of artificial neural networks to predict pyrite oxidation in a coal washing refuse pile. Fuel. 2013;104:163-169.
47. Hemmat Esfe M, Rostamian H, Reza Sarlak M, Rejvani M, Alirezaie A. Rheological behavior characteristics of TiO_2-MWCNT/10w40 hybrid nano-oil affected by temperature, concentration and shear rate: An experimental study and a neural network simulating. Physica E: Low-dimensional Systems and Nanostructures. 2017;94:231-240.
48. Program Committee of ICSE-SEIP 2019. 2019 IEEE/ACM 41st International Conference on Software Engineering: Software Engineering in Practice (ICSE-SEIP); 2019/05: IEEE; 2019.
49. Rashki S, Safardoust-Hojaghan H, Mirzaei H, Abdulsahib WK, Mahdi MA, Salavati-Niasari M, Khaledi A, Khorshidi A, Mousavi SG. Delivery LL37 by chitosan nanoparticles for enhanced antibacterial and antibiofilm efficacy. Carbohydrate Polymers. 2022;291:119634.